

Coherent polarimetric SAR simulation of maize

ZHANG Lu¹, LI Xinwu¹, DU Hejuan², MA Hongzhang², GUO Huadong¹

1. Key Laboratory of Digital Earth, Center for Earth Observation and Digital Earth, Chinese Academy of Sciences, Beijing 100101, China;

2. State Key Laboratory of Remote Sensing Science, Jointly Sponsored by the Institute of Remote Sensing Applications of Chinese Academy of Sciences and Beijing Normal University, Beijing 100101, China

Abstract: This paper constructs a realistic three-dimensional scene of maize, and develops a coherent scattering model to simulate the polarimetric Synthetic Aperture Radar (SAR) data by analyzing the structure characteristics of maize, especially considering the relative spatial position and orientation of maize leaves. The multi-angle, multi-polarization backscattering coefficients dataset acquired from the scatterometer are compared with that calculated from the simulated polarimetric SAR data, showing that the amplitude information simulated by the model is valid. The HH-VV, HH-HV, and VH-VV phase difference of the simulated data are analyzed, showing that the simulated phase information is valid. Besides, Polarization response method and Cloude *H*- α classification method are applied to validate the simulated PolSAR data from the viewpoint of scattering types.

Key words: PolSAR simulation, coherent scattering model, maize

CLC number: TP721.2 **Document code:** A

Citation format: Zhang L, Li X W, Du H J, Ma H Z and Guo H D. 2010. Coherent polarimetric SAR simulation of maize. *Journal of Remote Sensing*. 14(4): 621—636

1 INTRODUCTION

With all-weather, day-night imaging and penetrating the crops capability, Synthetic Aperture Radar (SAR) has become one of the major tools to retrieve parameters of crop and underlying ground surfaces, estimate the yield and monitor the crop growth (Guo, 2000). Recently, the retrieval of the key physical parameters of crops from polarimetric SAR data has become one of the important applications of SAR remote sensing. While some polarimetric SAR sensors, such as Alos_PalSAR, RadarSat-2 and so on, have been launched successfully recently, there are still difficulties to meet the aforementioned research demands for polarimetric SAR data with multi-frequency and multi-angle. Therefore the simulation of polarimetric SAR data is an effective way to study the method to extract the physical parameters of crops.

To simulate SAR data of crops, a necessary step is to construct a vegetation scattering model. Most of the early models belong to the incoherent scattering model, which can only simulate the amplitude of backscattering return. For example, Attema and Ulaby (1978) proposed the water cloud model of vegetation. Lang *et al.* (1983) firstly used distorted Bonn approximation method to study single-layer random medium. Sacchi *et al.* (1994) developed a microwave backscattering model aiming at the grass canopy. In these models, the vegetation medium was simplified in terms of a homogeneous random

medium (Karam & Fung, 1988; Ulaby *et al.*, 1990).

Coherent scattering models have a capability of gaining not only the amplitude but also the phase information of the backscattering return with different polarizations, which have gradually become the hotspot in the development of SAR model. Some scattering approximates provide a theoretical basis for constructing coherent scattering models and simulating polarimetric SAR data, such as truncated infinite cylinder approximation, GRG (generalized Rayleigh-Gans) approximation (Fung, 1994; Karam *et al.*, 1988), and Foldy-Lax approximation (Tsang *et al.*, 1985) and so on. Yueh *et al.* (1992) may be the first to address the coherence effects caused by the vegetation structure. Lin *et al.* (1999) realized the tree structure by using fractal theory and developed the coherent scattering model focusing on forests. Taking the soybean as example, Chiu and Sarabandi (2000) studied the coherent scattering model of the short branches vegetation during its whole growing season, and analyzed the difference between the C band and L band. Generally, coherent scattering models construct the three dimensional virtual vegetation based on the field survey, then stimulate SAR backscattering return information by means of superposition of scattering units or Monte Carlo sampling method (Thirion *et al.*, 2006). Cloude and Williams (2003, 2006) applied a coherent scattering model to simulate L band and P band polarimetric SAR data of forests.

The planting area of maize, an important grain crop, is about

Received: 2009-10-10; **Accepted:** 2010-01-26

Foundation: Natural Science Foundation of China (No. 40730525), 973 Basic Research Program of China (No. 2009CB723906).

First author biography: ZHANG Lu (1976—), male, Associate Professor. He received his Ph.D degree in SAR remote sensing from the Institute of Remote Sensing Applications, Chinese Academy of Sciences. His current research interests include information extraction and physical parameter estimation using Polarimetric SAR images. E-mail: luzhang@ceode.ac.cn

20 million hectares in China. However, because of the special structure of maize crop and the sensitivity of coherent scattering model to the structure, the existing polarimetric SAR simulation methods are not suitable for maize, especially for the leaves which are represented by a single shape, such as the elliptical thin disk. The relative spatial position and the orientation follow a random distribution. Considering the relatively large size of the maize leaf, a certain distribution of the orientation angle of maize leaf, and the variety of the orientation angle of a single leaf, the existing simulation methods are limited for maize leaf.

In this paper, a polarimetric SAR simulation for maize is developed that the relative spatial position and orientation of leaves are considered. The model accuracy is validated using backscatter measurements of a maize field obtained from the truck-mounted scatterometer and some polarimetric characteristics of maize. The new simulation method will provide theoretical and data supports for retrieving the physical parameters of maize.

2 COHERENT SIMULATION OF MAIZE

Considering the sensitive of the coherent scattering to the structure of observed targets, construction of realistic structures of maize is one of the significant issues to simulate the polarimetric SAR data. This paper proposes a strategy of constructing the realistic three-dimensional scene of maize, by analyzing the structure characteristics of maize, especially considering the relative spatial position and orientation of leaves.

2.1 Leaf realization and simulation

The length and width of the maize leaf, relative to its thin stem, is large, that indicates the significant contribution of leaves to the whole backscattering of maize. In addition, not only the orientation angles of leaves follow a certain distributing, but also the orientation angle of one single leaf is not constant. So, if the maize leaf is represented as a single shape and random orientation angle distribution, it is not suitable to simulate the coherent scattering.

In this paper, the realistic structures that reasonably describe the relative positions and orientation angle of the leaves are constructed. The leaves of maize are located evenly and directly at the stem, rather than the random location of the canopy of maize, because the maize only has a stem without branches. For the orientation angles of leaves, they are also no longer modeled as random distribution. Commonly, the orientation angle is represented in terms of the plane angle and altitude angle. The plane angle indicates the leaf direction in horizontal plan and follows the uniform distribution. The altitude angle is the angle between the orientation of the leaf and the normal line, namely leaf inclination angle. Generally, the inclination angle of a single maize leaf is not fixed and increases constantly from the leaf root to leaf tip. For the convenience of measurement and simulation, the leaf is divided into several sections. According to the field survey, (1) the inclination angle of each section is basically constant; (2) the inclination angles of sections with

the same serial number are close and follow the Gauss distribution. Therefore, only two parameters are needed to model the inclination angle of sections with the same serial number, namely the mean value and stand deviation.

In this coherent scattering model, the maize leaf is represented as a combination of several thin cuboids which are placed end to end. The orientation angle of a cuboid is decided by the plane angle and the inclination angle of the section which the cuboid represents. The structure of maize in this model is shown in Fig.1. So it can describe the spatial structure characteristics of maize leaves accurately. Leaf scattering is calculated in the GRG approximation (Ulaby & Elachi, 1990), which can reduce the calculation time effectively. The input parameters for simulating the leaf scattering include the length, the width, the thickness, the water content, the inclination angle of each segment, number of leaves in a maize, and so on.

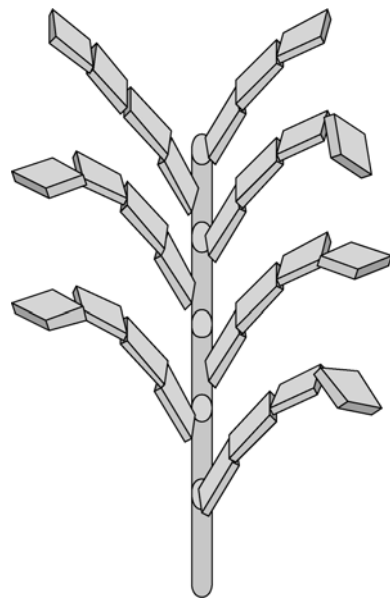


Fig. 1 Three-dimensional structure diagram of maize
(The stem is formed by some cylinders and the leaf is formed by some thin cuboids.)

2.2 Stems and ears realization and simulation

The stem of maize is basically vertical to the ground surface with little variety. The spatial location of the root of a stem is represented in terms of the plane coordinate and DEM where it lies. In this paper, the stems and the ears both are modeled as some thin cylinders. The truncated infinite cylinder approximation (Karam *et al.*, 1988) can be applied to drive the scattering solution. The dielectric constants of the stems, ears and the leaves are all simulated by dielectric models proposed by Elrayes & Ulaby (1987) and Ulaby & Elrayes (1987). The length, radius, water content and average number of maize plants per square meter of maize stem and ears are all necessary parameters of the model.

2.3 Ground surface realization and simulation

The earth's surface in this model is described as many small triangular facets. Every resolution cell is composed of many

facets with its own orientation to ensure fully-developed speckle. The model for surface scattering is two-scale, in which the small-scale model is used for each facet that adopts small perturbation model (SPM) to stimulate its backscattering information, and the larger-scale used to construct DEM and the location of each facet. For the dielectric constant of the ground surface, different dielectric models will be used in corresponding bands of electromagnetic wave (Dobson *et al.*, 1985; Hallikainen *et al.*, 1985). The roughness and volume moisture of ground surface are input parameters.

2.4 Attenuation simulation of the maize canopy

The attenuation, experienced by the electromagnetic wave propagating through the vegetation layer, is one of the major factors to affect the backscattering return. The higher the frequency is, the serious the attenuation will be. The effect of the attenuation must be considered when simulating the scattering of maize. The attenuation grids calculated from the three-dimension structure are used to account for scattering in this model. For the simulation of low or moderate resolution polarimetric SAR data, the attenuation in the same vegetation layer with the same height is similar. So, the same attenuation can be used in the vegetation layer with the same height for simplifying the computing progress. According to the structure characteristics of maize, a three layers structure is applied in this model and shown in Fig.2. The first layer (which is close to the ground surface), in the condition of no shot vegetation in the underlying surface, could be considered that there only exists stems, which is a very thin layer for maize. The second layer (middle layer) includes not only the stems but also the leaves and the fruits. The third layer mainly includes leaves, also the ears at some growing sections. The effective permittivity of each layer is constant, but may be different between the three layers, therefore resulting in the change of attenuation. Fig.3 shows the attenuation characteristics of the simulated SAR data of maize, with HH and VV polarizations, C and L band and 30° of incidence angle. The depth shown in Fig.3 indicates the distance from the upper surface of the vegetation, the attenuation coefficient 1 shows no attenuation, 0 shows complete attenuation.

From Fig.3, we can get the following characteristics of stimulated attenuation: (1) The attenuation in C band is larger than that in L Band, corresponding to the feature that the lower the frequency of electromagnetic wave is, the stronger the penetration will be. (2) When the incident angle is 30°, the attenuating at VV polarization is higher than that at HH polarization.

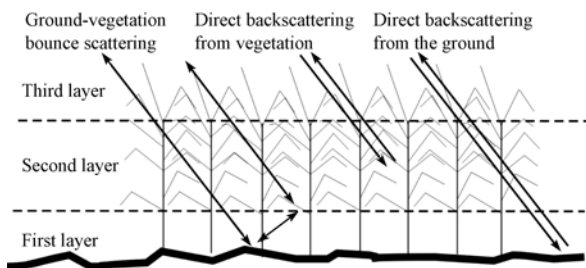


Fig. 2 Diagram of the scattering mechanism of the maize

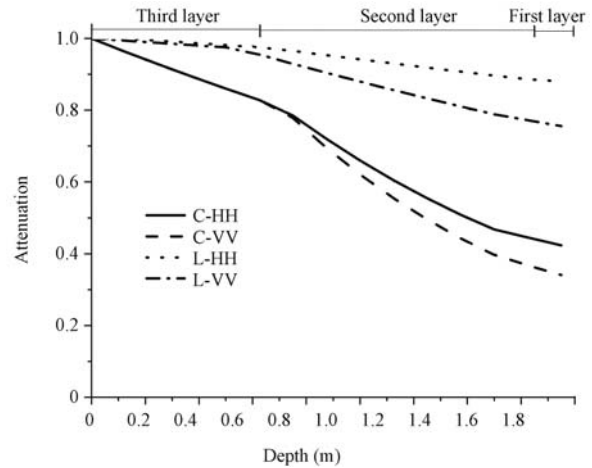


Fig. 3 Attenuation simulation of the maize (The incidence angle is 30°, the frequencies are C and L bands, the polarization stations are HH and VV.)

(3) The change trend at the two polarizations is different between the three layers, especially in C band. For example, the attenuation at VV polarization in the third layer is basically equal to that at the HH polarization, this is relative to the wider distribution of leaves' orientation; after entering the second layer, owing to the impact of maize stems, the attenuation trend at VV polarization will increase; when the electromagnetic wave propagates the first layer with only maize stems, the attenuation trend of HH polarization is decreased. Therefore, the location and orientation of stems and leaves will affect the attenuation at different polarization.

2.5 Simulation of the scattering mechanism

Three scattering mechanisms are considered for the coherent scattering model shown in Fig.2, which including:

- (1) direct backscattering from the underlying rough surface;
- (2) direct backscattering from vegetation;
- (3) ground-vegetation or vegetation-ground bounce scattering.

3 VALIDATION AND ANALYSIS OF SIMULATED RESULTS

To validate the coherent scattering model proposed in this paper, the amplitude and phase information of the simulated polarimetric SAR data will be validated respectively. In this section, we will use the backscattering coefficients acquired from the scatterometer to validate the amplitude of the simulated data, use the phase differences characteristics between typical polarizations to validate the simulated phase. In addition, the polarimetric response and the Cloud *H-α* classifier to validate the simulated SAR data from the scattering mechanism point of view.

3.1 Validation of the backscattering coefficients

A maize field near the Heihe River, China is chosen as study area. The HH and VV backscattering coefficients dataset was collected on July 2, 2008, from the scatterometer over a wide range of incidence angles. The picture of fieldwork using scatterometer is shown in Fig.4. The radar system input parameters used in the simulation method are shown in Table 1, which are

referred to RadarSat-2. The physical parameters dataset of the ground and maize (Table 2) were also collected as input parameters to simulate the polarimetric SAR data from different incidence angles (20°—60° at 10° increment) at C band by using this model. Fig.5 is the simulated polarimetric SAR RGB pseudo-color composite image, where red, green and blue represent the VV, HV and HH polarization respectively. The circle in the center of image indicates the maize, surrounded by bare soil.

Fig.6 and Fig.7 show the HH and VV simulated and measured backscattering coefficients by using the scatterometer versus incidence angle at C-band, respectively. From them, good agreement is obtained between the model predictions and measured backscattering coefficients. However, there still exists little deviation. One is that the backscattering coefficients acquired from scatterometer is more fluctuating compared with that of simulated polarimetric SAR data. The main reason is that the irradiated area of the scatterometer is smaller than that of the simulation, therefore the differences between the individual structures of maize will significant affect the backscattering coefficients acquired from the scatterometer, while the simulation results emphasizes the average effects. Besides, the measuring backscattering coefficients are larger relatively at high incidence angles, especially at VV polarization which is sensitive obviously to the incidence angle. This is caused by the



Fig. 4 Field measurement by using the scatterometer (Provided by University of Electronic Science and Technology of China - UESTC)

Table 1 Input parameters of simulated SAR system and the ground

Parameter	Value
Band	C(5.4GHz)
Resolution	15m×10m (azimuth×slant range)
Incidence angle	20°—60°
Platform altitude	798km
Roughness of ground	
Large-scale	2.5cm
Small-scale	0.25cm
Moisture of ground (mv)	20%

Table 2 Input parameters of the maize

Parameter	Value	Parameter	Value
Planting density	8/m ²	Leaf density	14 /plant
Plant height	175m	Lenth of leaf	0.6m
Lenth of stem	1.17m	Width of leaf	6.3cm
Radium of stem	1.45cm	Thickness of leaf	0.024cm
Moisture of stem (mg)	0.9	Mositure of leaf (mg)	0.75
Inclination angle of stem	0—5°	Inclination angle of leaf	
		Section 1	20 °
		Section 2	35 °
		Section 3	80 °

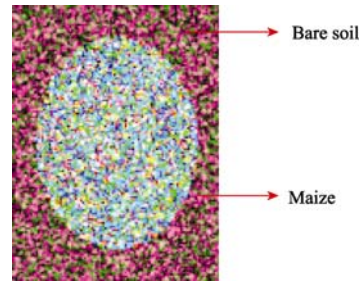


Fig. 5 Simulation POLSAR image of Maize (The incidence angle is 30°, the frequencies are C bands. Red: VV, Green: HV, Blue: HH.)

calibration error brought by increasing the measuring area of the scatterometer at high incidence angles. For all that, the simulated backscattering coefficients are in good agreement with the measuring data, which shows the simulated method is effective for maize.

3.2 Contribution from different scattering mechanisms

Fig.6—8 show the scattering contributions from different mechanisms versus incidence angle at HH, VV and HV typical polarizations by utilizing the simulated SAR data.

From Fig.6—8, we can see that there is little backscattering contribution from the ground at C band, due to the serious attenuation of the electromagnetic wave which propagating through the maize canopy, caused by the bloom simulated maize canopy and shorter wave length at C band. Therefore the scattering from the underlying ground surface will be reduced serious, especially at high incidence angles.

At C band, it is found that the VV backscattering coefficient is dominated by the direct scattering from the maize, comparing

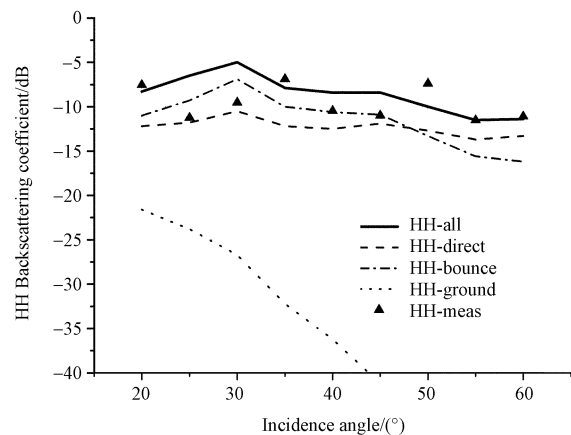


Fig. 6 HH backscattering coefficient of the maize

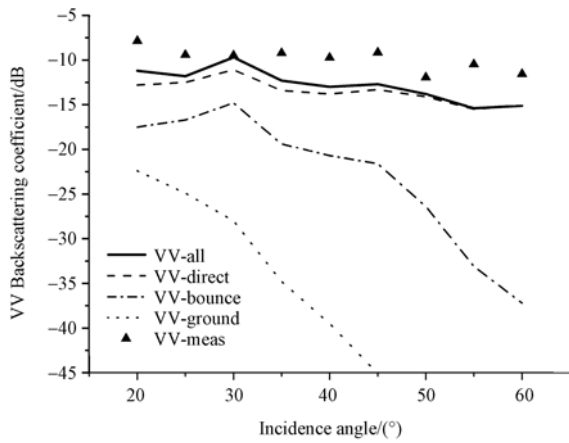


Fig. 7 VV backscattering coefficient of the maize

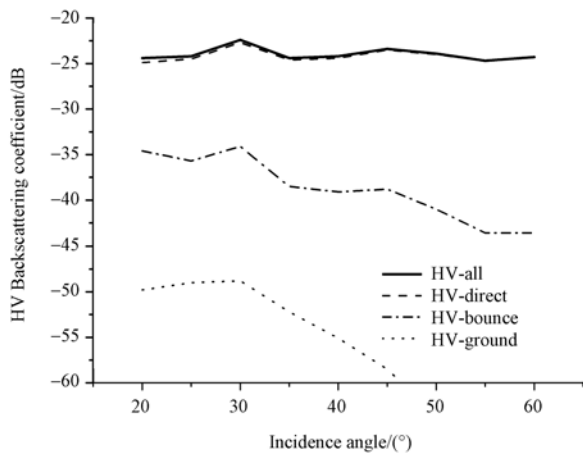


Fig. 8 HV backscattering coefficient of the maize

with contributions from direction scattering from ground and the bounce scattering from ground and maize, especially at high incidence angles. The reason is that bounce scattering at VV polarization will rapidly weaken when the incidence angle increases. At HH polarization, there is a comparable backscattering contribution from the direct scattering from maize and the bounce scattering, where the contribution from later mechanism is little larger than that from the former mechanism at low incidence angles, but at high incidence a significant contribution comes from the former mechanism. So, considering that the direct scattering from the maize has nothing to do with the ground surface, and it is dominated at VV polarization, the physical parameters of maize can be obtained from VV backscattering coefficients with little impact from the ground.

Besides, it is obvious that the cross-polarized HV scattering coefficient is dominated by the direct backscattering from the maize at C band. The cross-polarized scattering is the difficulty to be simulated. In this model, the cross-polarized scattering will be small because the multiple scatter from the vegetation is not under consideration. Another reason probably is the first-order approximation of ground-vegetation bounce scattering mechanism.

3.3 Validation of the phase

The advantage of the coherent scattering model is that it not only can obtain the scattering intensity of the observing objects, but also can acquire the phase information. The phase difference between different polarizations has a capability to reflect the characteristics of terrain objects represent by a special distribution, which can be used to verify the validation of the simulated phase. Fig. 9(a) shows the phase difference between

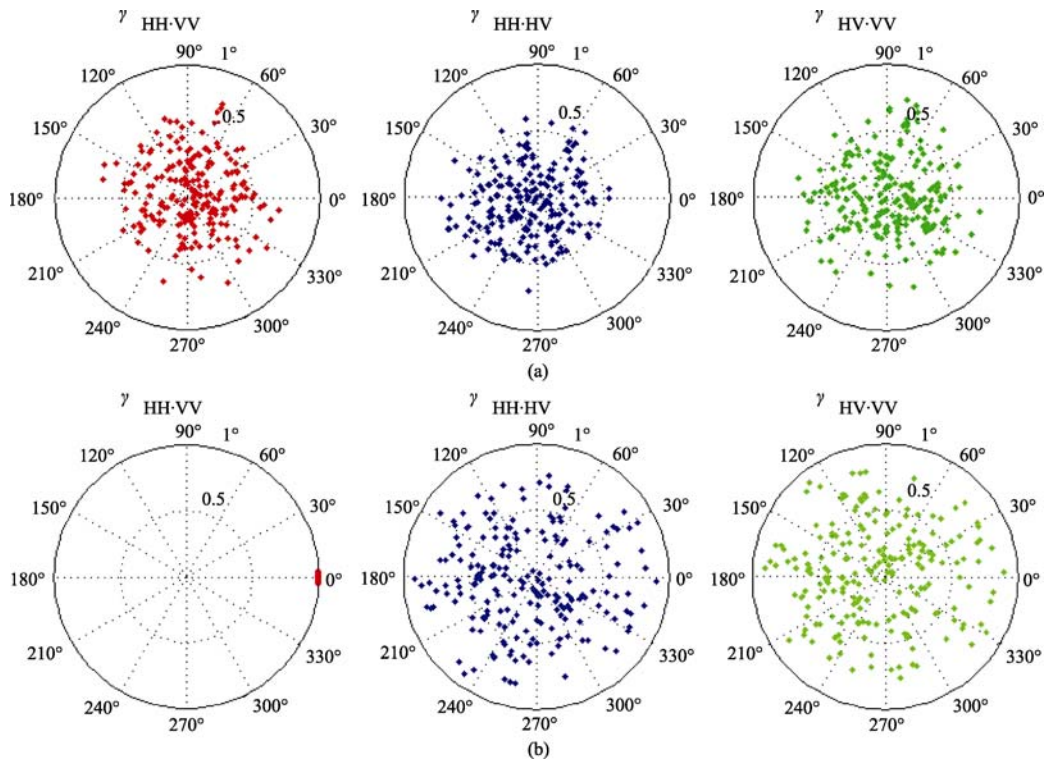


Fig. 9 Phase difference between typical polarizations (a) Maize; (b) Bare soil

some typical polarizations from the simulated SAR data of maize. From the figure, the phase differences between HH-VV, HH-HV and HV-VV of maize all perform as random distribution, which is identical to the phase characteristics of vegetation concluded by the field survey dataset (Ulaby & Elachi, 1990). Therefore, the simulated phase of maize is reliable. In addition, the phase difference of bare soil from the simulated polarimetric SAR data images is shown in Fig. 9(b), the simulated result shows that the HH-VV phase difference distributes in the vicinity of 0° , which also confirms the validation of the coherent scattering model in phase simulation.

3.4 Polarimetric response of simulated polarimetric SAR Data

The polarimetric response represents the backscattering coefficients with different polarizations by using the three-dimension diagram, which includes co-polarization response and cross-polarization response. The polarimetric response respects the backscattering power change of the observing targets in the

specific polarization combinations to a certain extent. Generally, the polarimetric responses are different for different types of observing objects, which can be used to validate the simulated polarimetric SAR data of maize. Fig.10 shows the co-pol responses and cross-pol responses from the simulated maize and bare soil. It is in agreement with that derived from the real polarimetric SAR data described by Ulaby and Elachi (1990).

3.5 Cloude H - α classification of simulated polarimetric SAR data

Cloude and Pottier (1997) developed a target matrix decomposition method from polarimetric SAR data, which can obtain the scattering types of terrain objects. Because the scattering type can be used to classify terrain objects, Cloude decomposition method can be used to validate the coherent scattering simulation proposed in this paper, by comparing the scattering type derived from the simulated SAR data of maize and bare soil with that of the typical terrain objects.

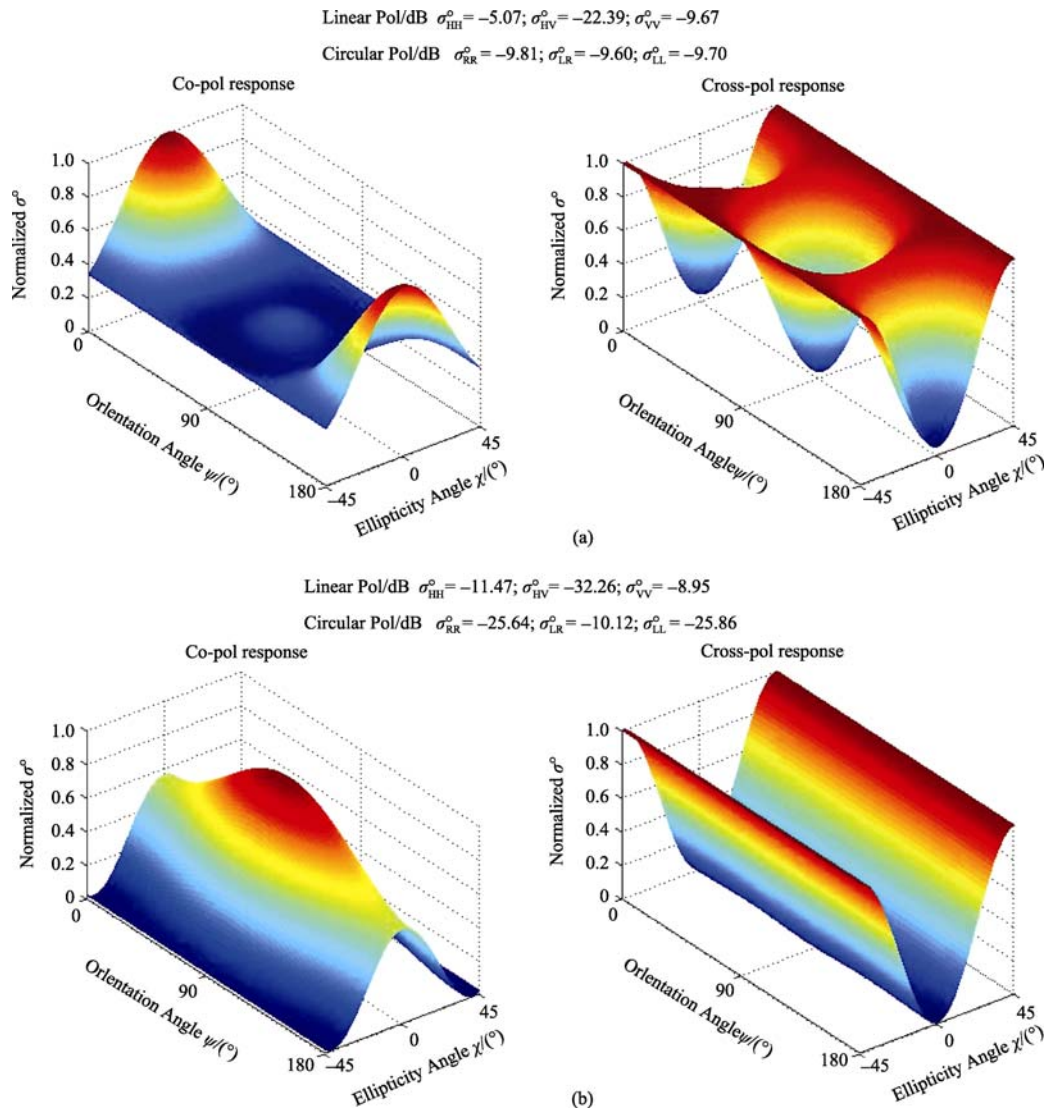


Fig. 10 Response of the simulated SAR data
 (a) Maize; (b) Bare soil

Fig.11 (a) is an H - α classification image of typical terrain objects. From this figure, the terrain objects can be classified into 9 different scattering types, between which the scattering type of vegetation located in the center region 5, while the scattering type of bare soil belongs to the region 7 which is located in the left down corner. Fig. 11 (b),(c) are H - α scatter diagram calculated from the simulated polarimetric SAR data

of maize and bare soil, respectively. It is clear that the H - α values of maize and bare soil are basically distributed in the region 5 and region 7, respectively, that better accords with the classification results of the typical objects on the ground in Fig.11 (a). Consequently, the results show the simulated polarimetric SAR data of maize is effective from the point of view of scattering types.

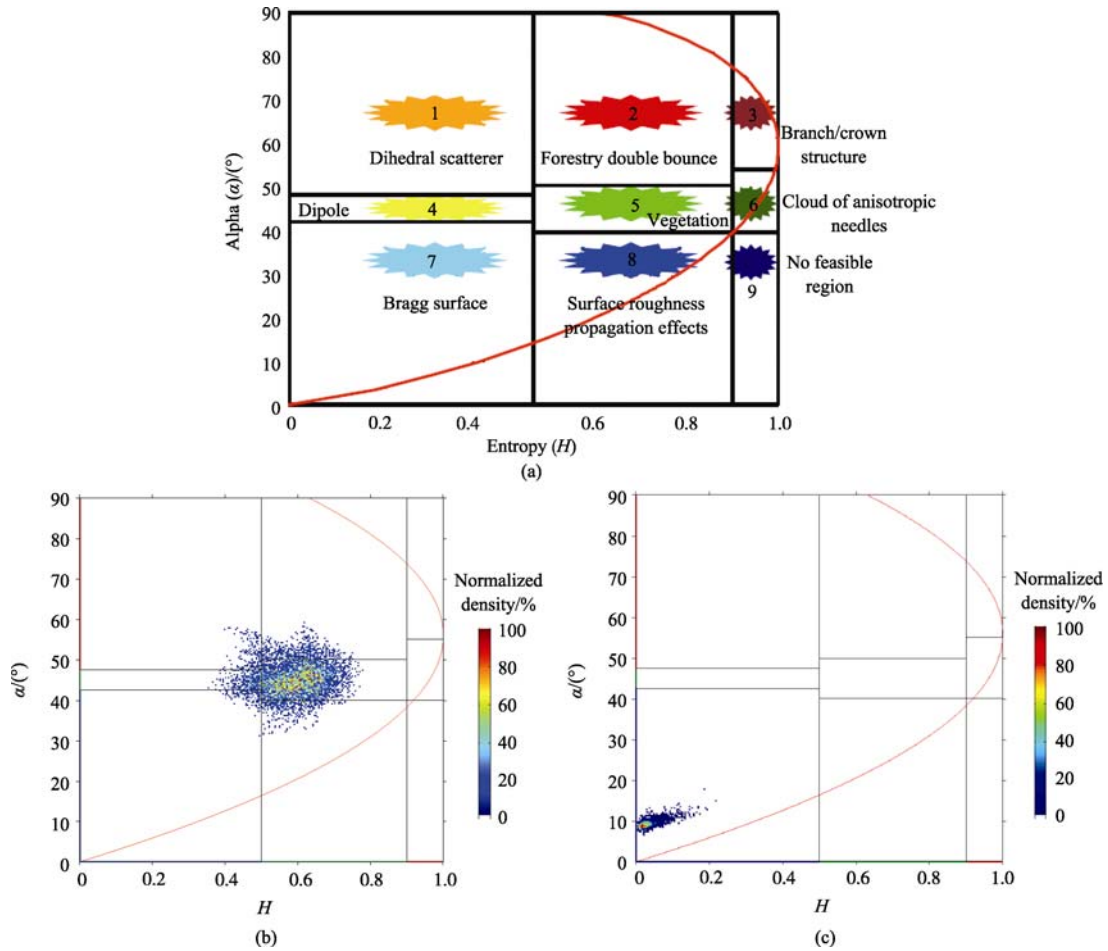


Fig. 11 Cloude H - α scatter diagram of the simulated SAR data
 (a) Maize; (b) Bare soil; (c) H - α classification map (Source: report of H - A - α theory from PolSARpro tool)

4 CONCLUSION

By analyzing the structure characteristics of maize, especially considering the relative spatial position and orientation of maize leaves, this paper constructs a realistic three-dimensional scene of maize, and develops a coherent scattering model of maize. In this model, the leaves of maize are located evenly and directly at the stem, rather than the random location of the canopy of maize. For the orientation angles of leaves, they are also no longer modeled as random distribution, but a certain distribution pattern. The maize leaf is divided into several sections, each of which is represented as a thin cuboids and allocated with corresponding inclination angle. Besides, the strategy of the attenuation and the scattering mechanisms are also discussed in this paper.

Taking the structure characteristic and physical parameters of maize collected from the field near Heihe river, China in July as input parameters, the polarimetric SAR data of maize over a wide range of incidence angles at C band will be simulated by using the coherent scattering model of maize. The multi-angle, multi-polarization backscattering coefficients dataset acquired from the scatterometer is compared with the simulated PolSAR data, showing that the amplitude information simulated by the model is valid. The HH-VV, HH-HV, and VH-VV phase difference of the simulated data are analyzed, showing that the simulated phase information is valid. Besides, polarization response method and cloude H - α classification method are applied to validate the simulated PolSAR data from the viewpoint of scattering types.

Acknowledgements: The authors would like to thank Hejuan Du and Jianguang Wen for their data support of field measurement dataset and scatterometer dataset of maize collected from the joint experiment of forest and arid area eco-hydrological in the middle reaches of Heihe, and Prof. Touzi for the PWSAR2 software support. The scattering approximations used in the polarimetric SAR simulation are realized based on the open-source PolSARPro software.

REFERENCES

- Attema E P W and Ulaby F T. 1978. Vegetation modeled as a water cloud. *Radio Science*, **13**(2): 357—364
- Chiu T and Sarabandi K. 2000. Electromagnetic scattering from short branching vegetation. *IEEE Transactions on Geoscience and Remote Sensing*, **38**: 911—925
- Cloude S R and Pottier E. 1997. An entropy based classification scheme for land applications of polarimetric sar. *IEEE Transactions on Geoscience and Remote Sensing*, **35**(1): 68—78
- Cloude S R and Williams M L. 2003. A coherent em scattering model for dual baseline polinsar. IGARSS2003: Learning from Earth's Shapes and Colours. Toulouse, France: Institute of Electrical and Electronics Engineers Inc
- Dobson M C, Ulaby F T, Hallikainen M T and Elrayes M A. 1985. Microwave dielectric behavior of wet soil .2. dielectric mixing models. *IEEE Transactions on Geoscience and Remote Sensing*, **23**(1): 35—46
- Elrayes M A and Ulaby F T. 1987. Microwave dielectric spectrum of vegetation .1. experimental-observations. *IEEE Transactions on Geoscience and Remote Sensing*, **25**(5): 541—549
- Fung A K. 1994. Microwave Scattering and Emission Models and Their Applications . London: Artech House
- Guo H D. 2000. Radar for Earth Observation: Theory and Applications. Beijing: Science Press
- Hallikainen M T, Ulaby F T, Dobson M C, Elrayes M A and Wu L K. 1985. Microwave dielectric behavior of wet soil .1. empirical-models and experimental-observations. *IEEE Transactions on Geoscience and Remote Sensing*, **23**(1): 25—34
- Karam M A and Fung A K. 1988. Electromagnetic scattering from a layer of finite length, randomly oriented, dielectric, circular-cylinders over a rough interface with application to vegetation. *International Journal of Remote Sensing*, **9**(6): 1109—1134
- Karam M A, Fung A K and Antar Y M. 1988. Electromagnetic wave scattering from some vegetation samples. *IEEE Transactions on Geoscience and Remote Sensing*, **26**(6): 799—808
- Lang R H and Sighu J S. 1983. Electromagnetic backscattering from a layer of vegetation: a discrete approach. *IEEE Transactions on Geoscience and Remote Sensing*, **21**(1): 62—71
- Lin Y C and Sarabandi K. 1999. A monte carlo coherent scattering model for forest canopies using fractal-generated trees. *IEEE Transactions on Geoscience and Remote Sensing*, **37**(1): 440—451
- Saatchi S S, Treuhalf R and Dobson M C. 1994. Estimation of leaf area index over agricultural areas from polarimetric sar images. IGARSS1994. Pasadena, CA, USA: IEEE, Piscataway, NJ, USA
- Thirion L, Colin E and Dahon C. 2006. Capabilities of a forest coherent scattering model applied to radiometry, interferometry, and polarimetry at p- and l-band. *IEEE Transactions on Geoscience and Remote Sensing*, **44**(4): 849—861
- Tsang L, Kong J A and Shin R T. 1985. Theory of Microwave Remote Sensing. New York: Wiley Series in Remote Sensing
- Ulaby F T and Elachi C. 1990. Radar Polarimetry For Geoscience Applications. Morwood, MA: Artech House
- Ulaby F T and Elrayes M A. 1987. Microwave dielectric spectrum of vegetation .2. dual-dispersion model. *IEEE Transactions on Geoscience and Remote Sensing*, **25**(5): 550—557
- Ulaby F T, Sarabandi K and McDonald K, et al. 1990. Michigan microwave canopy scattering model. *International Journal of Remote Sensing*, **11**(7): 1223—1253
- Williams M L. A Coherent, Polarimetric SAR Simulation of Forests for PolSARPro - Design document and algorithm specification. 2006
- Yueh S H, Kong J A, Jao J K, Shin R T and Le T T. 1992. Branching model for vegetation. *IEEE Transactions on Geoscience and Remote Sensing*, **30**(2): 390—402

玉米作物极化 SAR 数据模拟

张 露¹, 李新武¹, 杜鹤娟², 马红章², 郭华东¹

1. 中国科学院 对地观测与数字地球科学中心 数字地球重点实验室, 北京 100101;

2. 中国科学院 遥感应用研究所 遥感科学国家重点实验室, 北京 100101

摘 要: 通过重点研究玉米叶子的空间位置、指向角分布, 分析玉米作物的结构特点, 建立玉米的三维结构模型和场景, 发展针对玉米作物的极化合成孔径雷达(synthetic aperture radar, SAR)数据模拟方法。利用该模拟方法和实地获取的玉米参数模拟极化 SAR 数据, 通过与散射计实地测量的多极化、多角度后向散射系数进行对比, 表明该模拟方法能够有效的模拟玉米作物的后向散射系数; 通过分析模拟极化 SAR 数据获得的 HH-VV、HH-HV、VH-VV 之间的相位差, 表明该模拟方法能够有效的模拟玉米作物散射的相位信息; 通过分析模拟数据的极化响应图和 Cloude H- α 分类图, 从散射类型角度验证了模拟极化 SAR 数据的有效性。

关键词: 极化 SAR 模拟, 相干散射模型, 玉米

中图分类号: TP721.2 **文献标识码:** A

引用格式: 张 露, 李新武, 杜鹤娟, 马红章, 郭华东. 2010. 玉米作物极化 SAR 数据模拟. 遥感学报, 14(4): 621—636

Zhang L, Li X W, Du H J, Ma H Z and Guo H D. 2010. Coherent polarimetric SAR simulation of maize. *Journal of Remote Sensing*, 14(4): 621—636

1 引 言

合成孔径雷达(synthetic aperture radar, SAR), 由于其特有的全天时, 全天候系统成像, 以及对农作物的穿透探测能力, 已经成为农作物信息获取、估产和长势监测的重要工具(郭华东, 2000)。近年来, 利用极化 SAR 数据获取植被和农作物关键信息已经成为 SAR 遥感的重要研究领域。越来越多的 SAR 系统具有了获取极化 SAR 数据的能力, 例如 ALOS-PALSAR(L 波段), RADARSAT-2(C 波段), 然而这些数据远不能满足农作物 SAR 遥感研究所需要的多频率、多角度数据要求。极化 SAR 数据模拟是研究农作物信息反演方法的重要途径。

SAR 数据的模拟需要建立散射模型。早期的植被模型多为非相干散射模型, 仅能模拟所研究植被的后向散射强度信息, 不具备模拟相位信息的能力, 无法用来模拟极化 SAR 数据。例如 Attema 和 Ulaby (1978) 提出水云模型, Lang 和 Sighu (1983) 提出的基于变形波恩近似的单层随机离散介质模型, Sacchi 等(1994)提出的针对草冠层的微波后向散射模型等。

这些模型通常将植被简化为均匀随机介质(Karam & Fung, 1988; Ulaby 等, 1990)。

相干散射模型具有获取各种极化方式下相位信息的能力, 已经成为当前 SAR 模型发展的热点。一些电磁波散射近似方法为相干散射模型的建立和极化 SAR 数据模拟提供了理论基础。例如截断的无限圆柱体近似, 瑞利金斯 GRG(generalized Rayleigh-Gans)近似(Fung, 1994; Karam 等, 1988), 以及 Foldy-Lax 近似(Tsang 等, 1985)等。Yueh 等(1992)最早研究了植被层的相干效果。Lin 和 Sarabandi(1999)利用分形理论实现了树的结构, 建立针对森林的相干散射模型。Chiu 和 Sarabandi(2000)以大豆为例研究短枝植被整个生长期的相干散射模型, 并对比了 C 波段和 L 波段的差别。相干散射模型通常根据地面调查数据生成虚拟三维植被景观, 然后通过对不同散射单元的叠加或者通过 Monte Carlo 采样方法模拟雷达后向散射的信息(Thirion 等, 2006)。Cloude (2003)和 Williams(2006)利用相干散射模型建立了 L 到 P 波段多种树木的极化 SAR 数据的模拟方法。

玉米在中国的种植面积有 200 万 hm^2 左右, 是

收稿日期: 2009-10-10; 修订日期: 2010-01-26

基金项目: 国家自然科学基金(编号: 40730525)和国家 973 计划(编号: 2009CB723906)。

第一作者简介: 张露(1976—), 男, 2008 年毕业于中国科学院遥感应用研究所, 获博士学位; 目前主要从事微波遥感方面的研究工作。E-mail: luzhang@ceode.ac.cn.

中国重要的粮食作物。由于玉米作物的结构特点以及相干散射模型对结构的敏感性, 现有的极化 SAR 模拟方法无法满足玉米作物模拟的需求, 尤其是对玉米叶子的模拟。现有模型通常将叶子视为一个单一的形状, 其指向和空间位置采用随机分布, 玉米叶子尺度大, 叶子指向有一定的分布规律, 且单个叶子的指向也存在变化, 这些表现出现有模拟方法在玉米模拟中的局限性。

2 玉米作物相干散射模拟

考虑到相干散射对目标结构的敏感性, 玉米场景建立的真实度是极化 SAR 数据模拟的关键之一。通过分析玉米的结构特征, 提出针对玉米的真实场景建立策略, 重点考虑了玉米叶子空间相对位置和指向角特征。

2.1 玉米叶子的散射模拟

玉米的叶子是玉米作物非常重要的组成部分, 相对于其细小的秆而言, 玉米叶子的长度和宽度具有较大的尺寸, 这些决定了叶子对玉米作物后向散射贡献的重要性。另外, 玉米叶子指向有一定的分布规律, 且单个叶子的指向也存在变化, 这些表明对于玉米叶子的相干散射模拟, 不能再将叶子视为单一形状, 且叶子的指向也不能采用随机分布, 应遵循一定的分布规律。

本文对叶子进行了较细致的三维模拟。重点考虑叶子的空间位置、指向角分布。对于空间位置, 由于玉米作物只有秆, 没有枝, 本文将叶子的基点直接均匀分布在玉米秆上, 而不是通常模型所采用的在冠层中随机分布。对于叶子指向角, 不再描述为随机分布, 而是符合一定的规律。玉米叶子的空间指向可以用球坐标系中的平面角和高度角来描述。平面角表示叶子的水平指向, 该角度具有均匀分布的特点。高度角表示叶子法线方向的夹角, 即叶倾角。通常, 单个玉米叶子的倾角并非是固定的, 从叶根到叶尖不断增大。为方便测量与模拟, 将叶子从叶根到叶尖分为多个子段, 并对每段进行编号, 根据实地测量结果, 得出: (1) 段内叶子的倾角基本固定; (2) 具有相同编号的叶子段的倾角相近, 并符合高斯分布。利用这一特点, 在模拟玉米叶子倾角时, 相同编号叶子段只需提供其平均值和标准差即可。

本模型将叶子简化为几个薄的长方体组合, 每个长方体代表一段叶子, 并且前后相连, 其指向由叶子的平面角和不同段的倾角确定, 如图 1。可以较

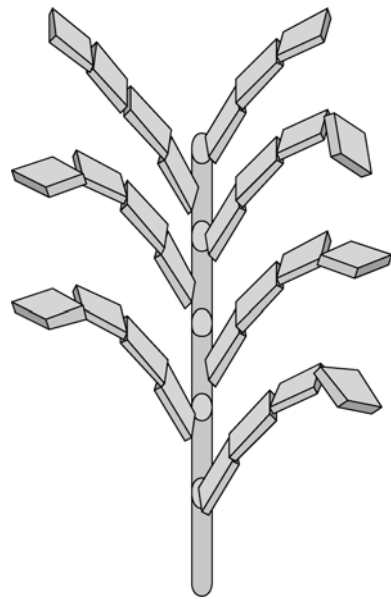


图 1 玉米植株三维几何模型结构示意图
(玉米秆由细长圆柱体构成, 叶子由薄长方体构成)

准确的描述玉米叶子的空间结构特点。叶子采用 GRG(Rayleigh Gans)近似方法(Ulaby & Elachi, 1990)模拟, 能够提高运算速度。叶子模拟需要提供的输入参数较多, 包括叶子的长度, 宽度, 厚度, 水含量, 叶子各段的倾角的分布, 以及每株玉米的叶子个数等等。

2.2 玉米秆和玉米穗散射模拟

玉米的秆基本垂直于地表, 仅在小角度范围内波动, 根部的空间位置由所在位置的平面坐标和地表高度确定, 本模型将玉米秆分为多个细长的圆柱体, 穗与秆一样, 同样被描述为细长的圆柱体。对于玉米的秆和穗, 本模型采用截断的无限长圆柱体近似(Karam 等, 1988)进行模拟。玉米秆、穗、以及叶子的介电常数均由(Elrayes & Ulaby, 1987; Ulaby & Elrayes, 1987)介电模型模拟。玉米的秆和穗的长度、半径、水含量以及每平方米平均的玉米株数是模型所需要的参数。

2.3 地表相干散射模拟

本模型中的地表被描述为许多小平面, 每个分辨率单元都由众多的不同方向的小平面组成以确保斑点噪声的完全发育。地表的粗糙度模拟采用双尺度模型, 小尺度用来描述单个小平面的粗糙度, 采用小扰模型(small perturbation model, SPM)模拟其散射信息, 大尺度粗糙度建立数字高度模型(DEM)并确定小平面的位置。对于地表的介电常数, 不同的波段将采用相应的介电模型(Dobson 等, 1985;

Hallikainen 等, 1985)获取。粗糙度和地表体积湿度是模拟地表需要提供的输入参数。

2.4 玉米冠层衰减的模拟

电磁波经过玉米植被层会发生衰减, 这是影响后向散射的主要因素, 且频率越高, 衰减越严重。模拟时需要考虑玉米植被层的衰减作用, 本模型根据玉米的植被层三维结构模型建立衰减网格, 对于中低分辨率的模拟, 相同高度的植被层衰减之间的变化不大, 可以假设相同高度的衰减一致, 简化运算过程。根据玉米的结构特点, 对衰减的模拟采用多层的策略, 通常分为 3 层, 如图 2, 第 1 层(靠近地表层), 在不考虑地表杂草的情况下, 可以认为只有秆的存在, 对于玉米, 这层很薄; 第 2 层(中间层)即包括玉米秆, 还包括叶子, 玉米成熟的时候还包括玉米的果实; 第 3 层主要是叶子, 一定时期包括玉米穗。每层内具有相同的有效介电常数, 但不同层次之间的介电常数存在差异, 因此导致衰减程度的变化。图 3 是 C 波段和 L 波段情况下, HH 和 VV 极化方式的衰减程度的变化图(入射角为 30°), 图中深度表示从植被的最高处向下的深度, 衰减程度 1 表示没有衰减, 0 表示完全衰减。

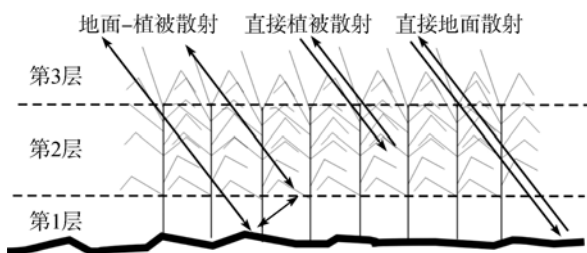


图 2 玉米散射分量及分层示意图

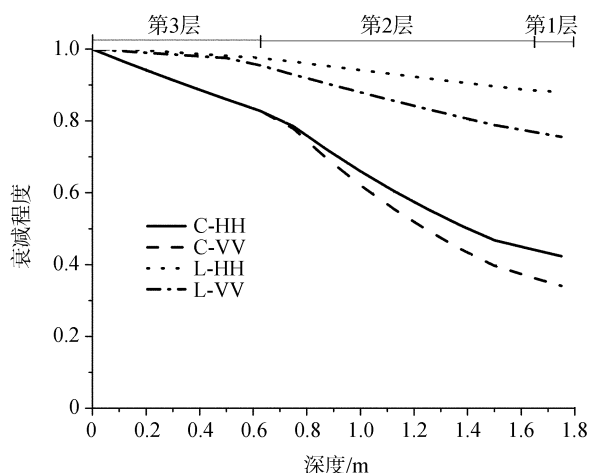


图 3 玉米植被层衰减程度模拟
(C, L 波段 HH, VV 极化方式, 入射角 30°)

从图 3 可以得出模拟出的衰减有如下特点: (1) C 波段的衰减大于 L 波段的衰减, 符合电磁波频率越低, 穿透性越强的特征; (2) 入射角为 30° 时, VV 极化方式的衰减程度大于 HH 极化方式的衰减程度。(3) 不同层次之间两种极化方式的衰减程度变化同样存在差异, 在 C 波段情况下更加明显。例如, 在第 3 层附近, 即没有秆的叶子层, VV 的衰减与 HH 的衰减基本相当, 这是由于叶子方向在较广的范围内均匀分布; 随着深度的增加, 进入到第 2 层后, 由于玉米秆的影响, VV 的衰减程度将增加; 当进入第 1 层后, 此时仅有玉米秆存在, HH 衰减的趋势将有所减少。因此, 秆、叶子的位置和方向性将共同影响不同极化的衰减程度。

2.5 模型中涉及的散射分量

本文建立的相干散射模型主要需要考虑以下 3 种散射类型分量的贡献, 包括地表的直接散射、玉米植被层的直接散射以及地表-玉米植被之间的二次散射, 如图 2。

3 模拟结果验证与分析

为验证本文提出的玉米相干模型的准确性, 需要对该模型模拟的极化 SAR 数据的强度和相位信息进行验证。

3.1 极化 SAR 模拟数据的后向散射系数验证

选择黑河实验区 2008-07-02 的玉米作物作为模拟对象, 利用散射计获取 C 波段, HH 和 VV 两种极化方式, 不同入射角的后向散射系数, 工作图像如图 4。根据实验区实地获取的地表及玉米结构参数, 利用本文提出的针对玉米作物的相干散射模型, 模拟 C 波段, 不同入射角的极化 SAR 数据(20° — 60° , 间隔 10°), 模拟采用的输入参数如表 1 和表 2, 分别是选用的雷达系统输入参数、地表参数, 以及玉米的相关参数, 其中雷达系统参数参照 RadarSat-2 相关参数。模拟得到的极化 SAR 数据合成图如图 5, 红色代表垂直极化方式 VV, 绿色代表交叉极化方式 HV, 蓝色代表水平极化方式 HH, 图中间部分为玉米作物, 周边是裸土。

提取模拟数据的 HH 和 VV 极化方式多角度后向散射系数, 与散射计测量结果进行对比。结果分别如图 6 和图 7, 其中, 实线表示模拟结果, 三角表示实地利用散射计获得的后向散射系数。通过对比, 模拟得到的不同角度的后向散射系数与实地散射计测量的后向散射系数能够较好的吻合, 但也存在一定的差异, 主要表现在: (1) 散射计得到的结果随角



图4 散射计测量工作照片
(由电子科技大学提供)

表1 模拟雷达系统及地表输入参数

参数	数值
波段	C(5.4GHz)
分辨率	15m×10m(方位向×斜距)
入射角	20°—60°
平台高度	798km
地表粗糙度	
大尺度	2.5cm
小尺度	0.25cm
地表湿度(mv)	20%

表2 玉米植被输入参数
(平均值, 2008年7月上旬 黑河地区玉米)

参数	数值	参数	数值
种植密度	8 株/m ²	叶子密度	14 片/株
株高	175m	叶子长度	0.6m
秆长度	1.17m	叶子宽度	6.3cm
秆半径	1.45cm	叶子厚度	0.024cm
秆湿度(mg)	0.9	叶子湿度(mg)	0.75
秆倾角	0—5°	叶子倾角	
		1 段	20°
		2 段	35°
		3 段	80°

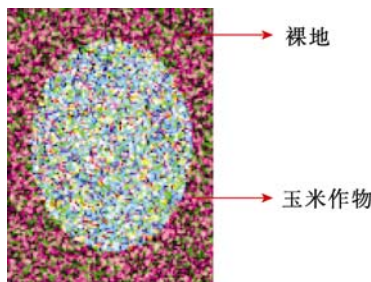


图5 玉米模拟极化 SAR 图像彩色合成图
(红: VV 绿: HV 蓝: HH C 波段, 入射角 30°)

度的变化明显, 其主要原因是由于散射计所照射的范围小于模型模拟的范围, 玉米个体结构差异会对其结果产生较大的影响, 模拟的范围大, 强调的是平均结果; (2) 在大入射角时, 散射计得到的后向散射系数相对较大, 在 VV 极化方式时更加明显, 这与大入射角时, 散射计测量面积增大带来的定标误差有一定的关系。总之, 模拟的后向散射系数基本与实测结果吻合, 说明该模拟方法的有效性。

3.2 典型散射类型分量的贡献分析

利用上述模拟结果分析 HH、VV 和 HV3 种极化方式, 不同入射角时, 多种典型散射分量对后向散射系数的贡献, 包括地表直接散射(ground)、玉米植被直接散射(direct)和地表-植被二次散射(bounce)三种散射类型分量。模拟结果如图 6—图 8。

根据图 6—图 8, 表明 C 波段时, 地表直接散射的贡献很小, 这是由于所模拟的玉米冠层很密, 而 C 波段的波长较短, 因此电磁波被在玉米冠层衰减很严重, 因此位于冠层最下层的地表散射被严重衰减, 并且随着角度的增加, 衰减会不断增强, 回波能量也就越来越弱。

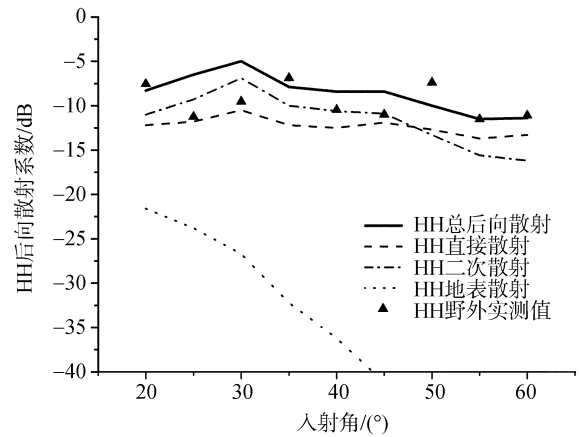


图6 HH 极化方式不同角度后向散射系数

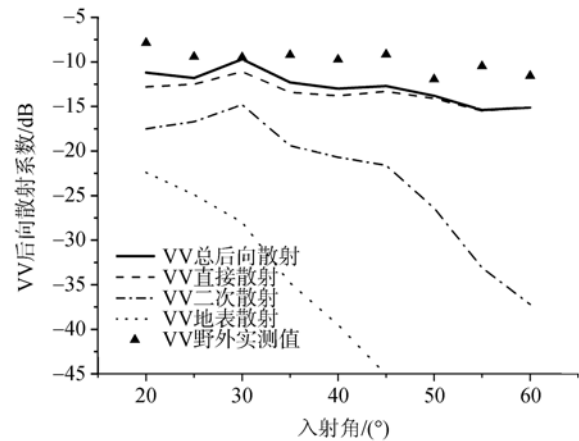


图7 VV 极化方式不同角度后向散射系数

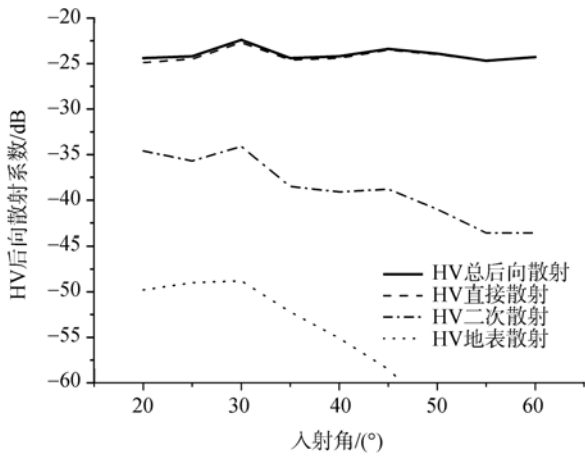


图 8 HV 极化方式不同角度后向散射系数

C 波段时, 对于 VV 极化方式, 相对于二次散射分量和地表散射分量而言, 玉米的直接散射分量对 VV 总后向散射的贡献最多, 在大入射角时直接散射分量的主导地位更加明显, 即 VV 极化方式的总后向散射主要由玉米直接散射分量提供。这是由于 VV 极化方式的地表-植被二次散射随着角度的增加迅速减弱。对于 HH 极化方式, 玉米直接散射和地表-植被二次散射的贡献相当, 在小入射角时, 地表-植被二次散射较高, 而在大入射角时, 其贡献减弱, 玉米直接散射成为主要的散射分量。总之, 玉米的

直接散射分量在 VV 极化方式时占主导地位, 且与地表无关, 因此, C 波段时利用 VV 极化方式获取玉米植被参数可以有效的避免地表的影响。

对于 HV 交叉极化方式, 其后向散射主要来自玉米植被的直接散射, 其他散射分量的贡献很小。交叉散射是相干模拟的难点, 用本模型模拟时, 植被间的多次散射未考虑, 此外电磁波与地表的相互作用采用的是一阶近似, 减弱了交叉散射项。

3.3 极化 SAR 模拟数据的相位验证

相干散射模型的优势在于它不仅能够获取地物散射的强度信息, 同时还能够获取地物散射的相位信息。不同极化方式之间的相位差能够反映地物的特征, 不同地物的相位差具有特定的分布特点, 可以用来验证模拟 SAR 图像相位的有效性。根据前文模拟得到的玉米种植区的极化 SAR 图像, 计算几种典型极化方式之间的相位差, 如图 9(a), 根据图 9(a), 玉米作物的 HH-VV、HH-HV 以及 HV-VV 之间的相位差都表现为随机分布, 符合根据真实 SAR 数据总结出的植被相位结果(Ulaby & Elachi, 1990), 利用该相干模拟方法得到玉米作物的相位是有效的。用该模型模拟的裸地的相位差分布图如图 9(b), 模拟结果满足 HH 与 VV 之间的相位差在 0°附近分布的特点。验证了该模型地表相位模拟的有效性。

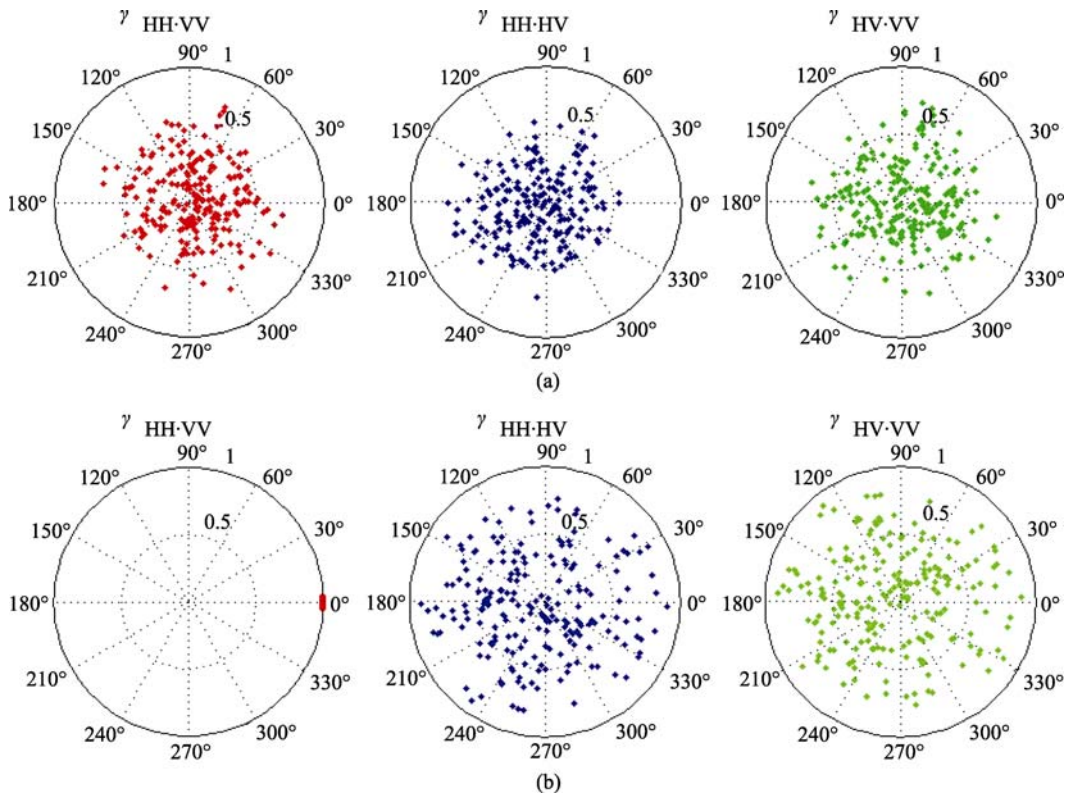


图 9 模拟数据典型极化方式相位差分布
(a) 玉米作物; (b) 裸土

3.4 极化 SAR 模拟数据的极化响应图分析

极化响应图是用三维图的形式将目标散射系数与极化状态之间的关系表示出来, 包括同极化响应图和交叉极化响应图。极化响应图在一定程度上反映了目标在特定极化方式组合下产生的回波功率的变化情况, 通常不同类型的目标回波具有不同形状的极化响应图, 可以用来验证极化 SAR 模拟数据的正确性。图 10(a)和图 10(b)分别是利用玉米作物区和裸地的极化 SAR 模拟数据计算得到的同极化和交叉极化响应图, 符合通过真实 SAR 数据得到的植被和裸地的响应图特点(Ulaby & Elachi, 1990)。

3.5 极化 SAR 模拟数据 Cloude $H-\alpha$ 分类图分析

针对极化 SAR 数据, Cloude 和 Pottier(1997) 提

出了目标矩阵分解方法, 该方法能够获取地物的散射类型。典型的地物具有固定的散射类型, 利用 Cloude 分解方法能够从玉米及裸地的极化 SAR 模拟数据获取物理散射类型信息, 并与典型地物散射类型图对比, 验证极化 SAR 模拟数据的有效性。

图 11(a)是典型地物 $H-\alpha$ 划分图, H 是散射类型的熵, 表现的是地物散射类型的随机程度, α 表现的是地物的散射类型。根据该图, 典型地物根据散射机制的不同, 被划分为 9 种类型, 其中植被位于图中的区域 5, 而裸地位于图中左下角的区域 7。图 11(b)和图 11(c)分别是根据玉米及裸地极化 SAR 模拟数据得到的 $H-\alpha$ 散点图, 根据该图, 玉米极化 SAR 模拟数据的 $H-\alpha$ 值基本分布在区域 5, 裸地极化 SAR 模拟数据的 $H-\alpha$ 值基本位于区域 7, 很好的

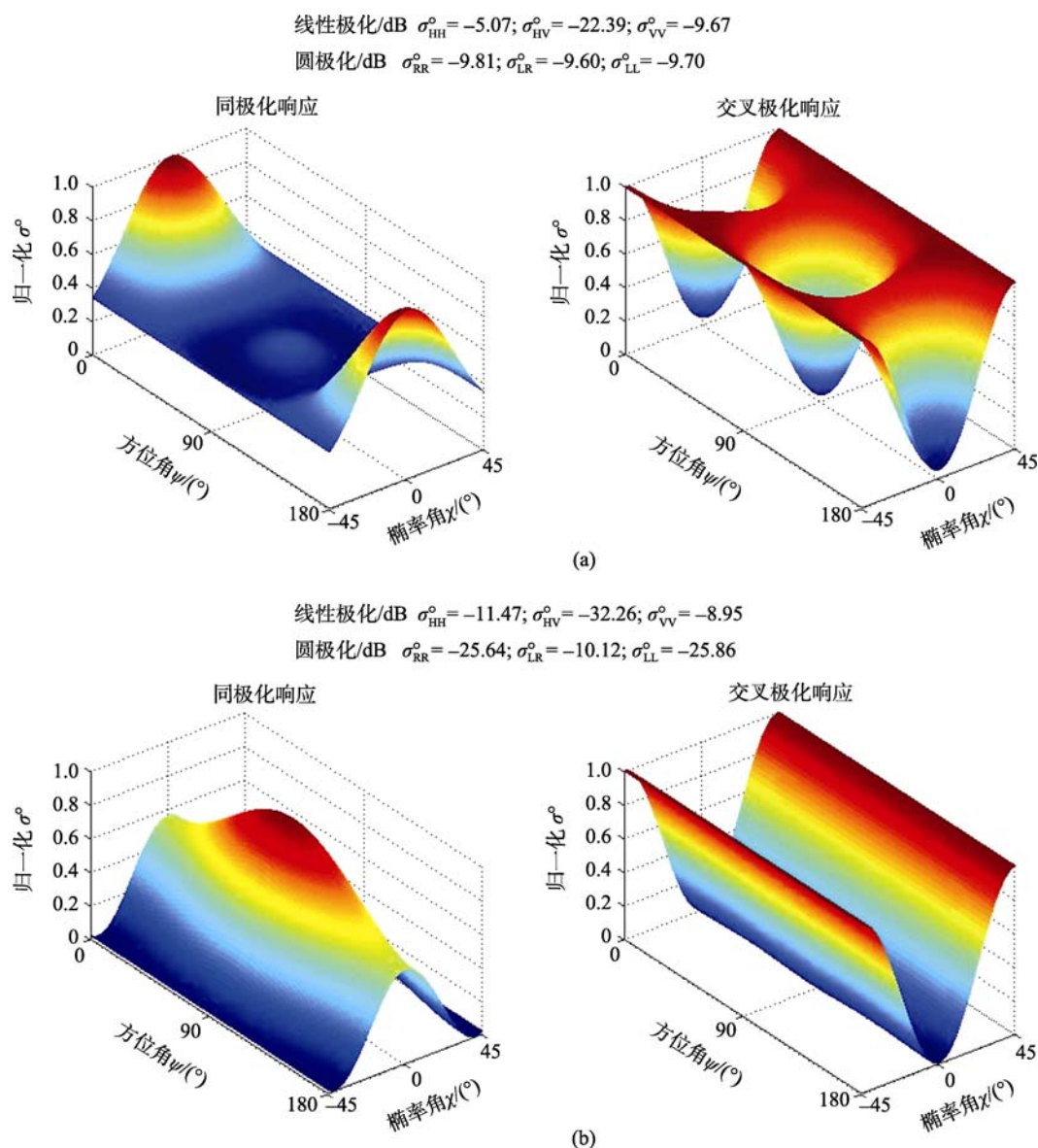
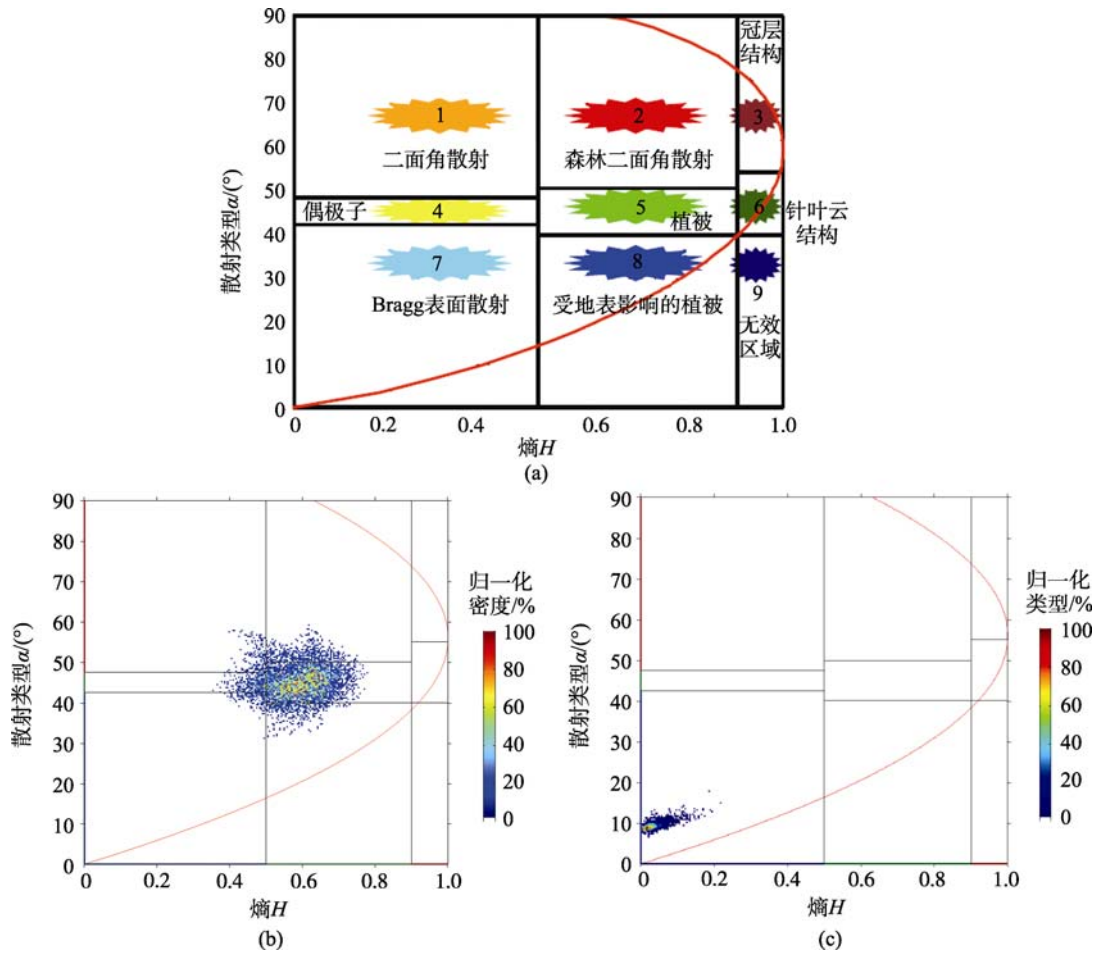


图 10 模拟数据响应图

(a) 玉米作物; (b) 裸土

图 11 模拟数据 Cloud $H-\alpha$ 分类图

(a) Cloud $H-\alpha$ 分类图(引自 PolSARpro 软件提供的 $H-A-\alpha$ 分解理论报告); (b) 玉米作物; (c) 裸土

符合图 11(a)中的典型地物的划分结果。从而从散射类型角度表明本文模拟的极化 SAR 数据是有效的。

4 结 论

本文通过分析玉米作物的结构特征, 建立符合玉米特征的三维结构模型, 重点考虑叶子的空间位置、指向角分布, 发展针对玉米作物的极化 SAR 数据模拟方法。

通过对玉米叶子空间位置的分析, 考虑玉米作物只有秆, 没有枝, 将玉米叶子的基点直接均匀分布在玉米秆上, 而不是通常模型所采用的在冠层中随机分布。对于叶子的指向角, 也不再被描述为随机分布, 而是符合一定的规律, 将玉米叶子分段处理, 每段叶子分配相应的叶子倾角。同时, 对衰减策略以及模拟中涉及的散射分量进行了讨论。

利用实地获取的 7 月份玉米结构, 物理参数模拟玉米作物的极化 SAR 数据, 并从后向散射系数、

相位以及散射类型角度验证玉米作物极化 SAR 模拟数据的有效性。结果表明: (1) 通过与散射计实地测量的多个角度后向散射系数进行对比, 证明了该模拟方法能够有效的模拟玉米作物的后向散射系数; (2) 对比模拟数据与典型地物极化间的相位差, 表明该模拟方法能够有效的模拟玉米作物散射的相位信息; (3) 通过分析极化 SAR 模拟数据的极化响应图和 Cloud $H-\alpha$ 分类图, 从散射类型角度验证了本文模拟的极化 SAR 数据的有效性。

致 谢 文中所使用的实地玉米作物结构数据以及散射计测量数据由黑河中游森林和干旱区生态水文联合试验提供, 感谢中国科学院遥感应用研究所杜鹤娟、闻建光的支持。文中极化 SAR 数据模拟方法中的散射近似方法在 PolSARPro 软件中提供的开源代码基础上开发; 极化 SAR 数据处理使用的 PWSR2 软件, 由加拿大遥感中心 Touzi 教授提供, 特此表示衷心的感谢。

REFERENCES

- Attema E P W and Ulaby F T. 1978. Vegetation modeled as a water cloud. *Radio Science*, **13**(2): 357—364
- Chiu T and Sarabandi K. 2000. Electromagnetic scattering from short branching vegetation. *IEEE Transactions on Geoscience and Remote Sensing*, **38**: 911—925
- Cloude S R and Pottier E. 1997. An entropy based classification scheme for land applications of polarimetric sar. *IEEE Transactions on Geoscience and Remote Sensing*, **35**(1): 68—78
- Cloude S R and Williams M L. 2003. A coherent em scattering model for dual baseline polinsar. IGARSS2003: Learning from Earth's Shapes and Colours. Toulouse, France: Institute of Electrical and Electronics Engineers Inc
- Dobson M C, Ulaby F T, Hallikainen M T and Elrayes M A. 1985. Microwave dielectric behavior of wet soil .2. dielectric mixing models. *IEEE Transactions on Geoscience and Remote Sensing*, **23**(1): 35—46
- Elrayes M A and Ulaby F T. 1987. Microwave dielectric spectrum of vegetation .1. experimental-observations. *IEEE Transactions on Geoscience and Remote Sensing*, **25**(5): 541—549
- Fung A K. 1994. Microwave Scattering and Emission Models and Their Applications . London: Artech House
- Guo H D. 2000. Radar for Earth Observation: Theory and Applications. Beijing: Science Press
- Hallikainen M T, Ulaby F T, Dobson M C, Elrayes M A and Wu L K. 1985. Microwave dielectric behavior of wet soil .1. empirical-models and experimental-observations. *IEEE Transactions on Geoscience and Remote Sensing*, **23**(1): 25—34
- Karam M A and Fung A K. 1988. Electromagnetic scattering from a layer of finite length, randomly oriented, dielectric, circular-cylinders over a rough interface with application to vegetation. *International Journal of Remote Sensing*, **9**(6): 1109—1134
- Karam M A, Fung A K and Antar Y M. 1988. Electromagnetic wave scattering from some vegetation samples. *IEEE Transactions on Geoscience and Remote Sensing*, **26**(6): 799—808
- Lang R H and Sighu J S. 1983. Electromagnetic backscattering from a layer of vegetation: a discrete approach. *IEEE Transactions on Geoscience and Remote Sensing*, **21**(1): 62—71
- Lin Y C and Sarabandi K. 1999. A monte carlo coherent scattering model for forest canopies using fractal-generated trees. *IEEE Transactions on Geoscience and Remote Sensing*, **37**(1): 440—451
- Saatchi S S, Treuhalf R and Dobson M C. 1994. Estimation of leaf area index over agricultural areas from polarimetric sar images. IGARSS1994. Pasadena, CA, USA: IEEE, Piscataway, NJ, USA
- Thirion L, Colin E and Dahon C. 2006. Capabilities of a forest coherent scattering model applied to radiometry, interferometry, and polarimetry at p- and l-band. *IEEE Transactions on Geoscience and Remote Sensing*, **44**(4): 849—861
- Tsang L, Kong J A and Shin R T. 1985. Theory of Microwave Remote Sensing. New York: Wiley Series in Remote Sensing
- Ulaby F T and Elachi C. 1990. Radar Polarimetry For Geoscience Applications. Morwood, MA: Artech House
- Ulaby F T and Elrayes M A. 1987. Microwave dielectric spectrum of vegetation .2. dual-dispersion model. *IEEE Transactions on Geoscience and Remote Sensing*, **25**(5): 550—557
- Ulaby F T, Sarabandi K and McDonald K, et al. 1990. Michigan microwave canopy scattering model. *International Journal of Remote Sensing*, **11**(7): 1223—1253
- Williams M L. A Coherent, Polarimetric SAR Simulation of Forests for PolSARPro - Design document and algorithm specification. 2006
- Yueh S H, Kong J A, Jao J K, Shin R T and Le T T. 1992. Branching model for vegetation. *IEEE Transactions on Geoscience and Remote Sensing*, **30**(2): 390—402

附中文参考文献

郭华东. 2000. 雷达对地观测理论与应用. 北京: 科学出版社